Morphodynamics of small-scale superimposed sand waves over migrating dune bed forms

Jeremy G. Venditti[1] and Michael Church

Department of Geography, University of British Columbia, Vancouver, British Columbia, Canada

Sean J. Bennett

Department of Geography, State University of New York at Buffalo, Buffalo, New York, USA

Received 2 July 2004; revised 2 June 2005; accepted 30 June 2005; published 29 October 2005.

[1] The kinematics and morphodynamics of low-amplitude, small-scale sand waves developed over migrating dunes are examined using data drawn from laboratory experiments. We refer to the superimposed features as "sand sheets," a general descriptive term for low-amplitude bed waves that are not easily classified as ripples, dunes, or bars. Within the experiments, the sheets formed downstream of the reattachment point at a distance that was invariant with dune size. Some sheets lacked slip faces composed of sand grains avalanching down a slope near the angle of repose. Over equilibrium dunes, three to four sand sheets were observed per 100 s. Sheet thickness was 10% of the height of the dune upon which they were superimposed; they migrated at 8 to 10 times the dune rate; they had nearly constant lengths over the full range of dune lengths and flow conditions; and they had aspect ratios of $\sim$0.025. Dunes and sand sheets represent distinct scales of sediment transport with different migration rates. However, sediment transport rates, calculated from the sand sheet and dune morphologies, are nearly identical. For transport equivalence to occur, sand sheets migrating at 10 times the dune rate must be 0.1 times the size, which is consistent with the morphological observations. Superimposed bed waves on dunes are often considered simply as additional roughness elements, but these results indicate that such bed waves are the agency by which the dune bed form itself moves downstream.

Citation: Venditti, J. G., M. Church, and S. J. Bennett (2005), Morphodynamics of small-scale superimposed sand waves over migrating dune bed forms, *Water Resour. Res.*, *41*, W10423, doi:10.1029/2004WR003461.

1. Introduction

[2] A wide variety of bed forms is known to develop at an assortment of scales under unidirectional flow in rivers. The hierarchical nature of bed forms in river channels has long been recognized [cf. *Jackson*, 1975]. Often two, three or even four distinct scales of bed form may occur in the same flow system [e.g., *Carey and Keller*, 1957; *Coleman*, 1969]. For example, ripples and dunes are frequently superimposed on bars [*Guy et al.*, 1966; *Coleman*, 1969; *Jackson*, 1976], ripples are commonly superimposed on dunes [*Guy et al.*, 1966; *Coleman*, 1969], and smaller dunes can be superimposed on larger dunes [*Pretious and Blench*, 1951; *Carey and Keller*, 1957; *Allen and Collinson*, 1974; *Jackson*, 1976]. Even bed load sheets [*Whiting et al.*, 1988] display this hierarchical nature because they are often found superimposed on bar forms [*Bennett and Bridge*, 1995] and dunes [*Whiting et al.*, 1988; *Livesey et al.*, 1998]. Several authors have reported superimposed bed forms where both scales are apparently in equilibrium with the flow [cf. *Pretious and Blench*, 1951; *Jackson*, 1976; *Rubin and McCulloch*, 1980], while others have suggested that, where channel discharges vary greatly, only one bed form scale is active [e.g., *Allen and Collinson*, 1974]. This latter interpretation of bed form superposition suggests that smaller scales are simply ancillary roughness elements and lag features associated with other flow conditions. *Allen* [1982] in particular has argued that only one scale of bed form is in equilibrium with the flow field at a given discharge and that other observed modes are formed by other flow stages.

[3] In this paper, we study the dynamics and kinematics of a bed form hierarchy composed of small-scale sand waves superimposed on larger-scale sand wave features. Both scales are in apparent equilibrium (not systematically changing their size, shape or migration rate in time or space) and both are simultaneously active in the channel. Although there have been many reports of bed form superposition, little research has been directed at examining the dynamics of multiple, superimposed equilibrium bed form scales in a single flow system. The paper describes experiments that display sand waves superimposed on dunes and how these distinct bed form scales interact through the agency of sediment transport.

[4] The issue of what terminology to apply to each bed form scale described in this paper is complicated. Despite well over a century of research on bed forms, there is no generally accepted classification scheme for the variety of forms observed. There is general agreement in the literature

[1] Now at Department of Earth and Planetary Sciences, University of California, Berkeley, California, USA.

0043-1397/05/2004WR003461$09.00

Table 1. Comparison of Bed Form Classification Schemes

Criteria	Ripple Definition	Dune Definition	Reference
Sediment caliber	can form when D < 0.6 mm only	can only form when D > 0.1 mm because of suspension threshold	*Inglis* [1949]; *Allen* [1982]
Flow roughness	can form when the flow is hydraulically smooth ($Re_g < 5$) only	can form when the flow is not hydraulically smooth ($Re_g > 5$)	*Liu* [1957]
Bedform shape or aspect ratio[a]	ripples are steeper than dunes and $h/l > 0.05$	$0.01 < h/l < 0.1$	*Guy et al.* [1966]; *Allen* [1968]
Relevant length scale	length scales with grain size $L = 1000D$ (later revised as $600-2000D$)	size scales with d ($H = d/6$; $L = 5d$)	*Yalin* [1964, 1985]
Excess shear stress	occurs when nondimensional excess shear stress (T) < 3 for D < 0.45 mm only	occurs at all other D in subcritical flow	*van Rijn* [1984]
Dimensional length	$l < 0.6$ m	$l > 0.6$ m	*Ashley* [1990]
Scaling with hydraulic parameters as in bed form existence diagrams	many threshold values	many threshold values	*Southard and Boguchwal* [1990]

[a]Note the overlap with ripple steepness. $Re_g = u_* D/\nu$ and $T = (\tau - \tau_c)/\tau_c$, where τ_c is the critical shear stress for sediment entrainment.

that there are at least two distinct bed form scales formed in sand under unidirectional, lower-regime flow; relatively small scale ripples and relatively large scale dunes (cf. reviews in work by *Allen* [1982] and *Ashley* [1990]). Yet, there is no unambiguous way to distinguish these two distinct bed form scales. Criteria to do so include (1) sediment caliber [*Inglis*, 1949], (2) hydraulic roughness [*Liu*, 1957], (3) bed form shape or aspect ratio (height/length, h/l [*Allen*, 1968]), (4) relevant length scale [*Yalin*, 1964], (5) dimensionless excess shear stress (transport stage [*van Rijn*, 1984]), (6) dimensional length [*Ashley*, 1990], and (7) scaling with hydraulic system parameters (velocity, depth, sediment size, Shields' nondimensional shear, stream power, Froude number) as in bed form existence diagrams (see reviews in work by *Allen* [1982] or the most recent versions of the existence fields in work by *Southard and Boguchwal* [1990] (Table 1). Complicating this issue, there are a great many cases that do not fit this simple dichotomization of lower-regime bed forms.

[5] It is tempting here to simply refer to the larger-scale forms as dunes and the smaller-scale forms as ripples. However, the smaller, superimposed bed form mode described here does not fit cleanly into the conventional classifications. Nevertheless, there is a need to give each mode some preliminary term to enable a clear presentation of the kinematics and dynamics of this bed form hierarchy. As such, the larger-scale bed form mode is given the preliminary term dune, as this mode fits most of the definitions given in Table 1, and the smaller-scale features are given the preliminary term "sheet," which is a general term that serves to describe very low amplitude bed topography. *Whiting et al.* [1988], *Dietrich et al.* [1989], and *Bennett and Bridge* [1995] define a specific species of sheet, the bed load sheet which has been linked to sediment sorting in heterogeneous sediments. Our description of sheets is in the spirit of the term and is prefaced by "sand" to explicitly acknowledge the distinction from bed load sheets formed in heterogeneous sediments. Further discussion of this terminology is given below.

2. Experimental Procedures

[6] The experiments were conducted at the USDA-ARS National Sedimentation Laboratory using a tilting recirculating flume 15.2 m long, 1 m wide, and 0.30 m deep. The flume was filled with ~2250 kg of washed and sieved white quartz sand with a median grain diameter $D_{50} = 0.5$ mm (Figure 1).

[7] Bed form development was observed over five separate flow stages (referred to as flows A through E; see Table 2). Flow depth d was ~0.15 m and mean flow velocities $\overline{U}$ ranged between 0.35 and 0.50 m s^{-1}. Froude and Reynolds numbers indicate that the flow was both subcritical and fully turbulent. These hydraulic conditions plot in the 2-D dune field on the bed form phase diagram of

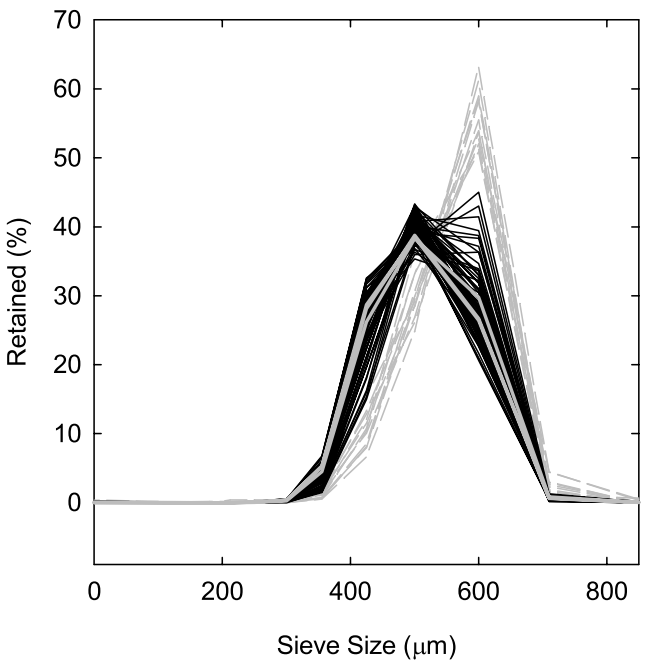

Figure 1. Grain size distributions of sand used in the experiments. Displayed are the bulk distributions (thick solid gray lines) and 109 Helley-Smith bed load samples (black lines). The twelve bed load size distributions that peak at 0.600 mm (thin dashed gray lines) were all from extremely small samples in which the true mode (and median) lies very close to, or on, the boundary between two sieve classes in a $^1/_4$ phi sieve stack.

Table 2. Summary of Initial Flow Parameters[a]

Flow Parameter	Flow A	Flow B	Flow C	Flow D	Flow E
			Values Based on Direct Measurements		
d, m	0.152	0.152	0.153	0.153	0.153
$\overline{U}$, m s^{-1}	0.501	0.477	0.454	0.399	0.356
Fr	0.411	0.391	0.370	0.326	0.290
Re	75936	72331	69568	61093	54580
Q, m^3 s^{-1}	0.0759	0.0723	0.0696	0.0611	0.0546
$S \times 10^{-4}$	12	11	7.0	5.5	5.5
			Determinations Based on Law of the Wall Using Lower 20% of Velocity Profiles		
u_*, m s^{-1}	0.030	0.026	0.022	0.017	0.016
τ, Pa	0.902	0.650	0.481	0.291	0.242
ff	0.029	0.023	0.019	0.015	0.015
Re_g	15	13	11	9	8
$(\tau-\tau_c)/\tau_c$	2.2	1.3	0.70	0.03	−0.15

[a]Velocity data are derived from measurements taken with a 300-mW Dantec Laser Doppler Anemometer (see *Venditti* [2003] for details). $Fr = \overline{U}/(gd)^{0.5}$, $Re = d\overline{U}/\nu$, $ff = 8\tau/\rho\overline{U}^2$, $u_* = (\tau/\rho)^{0.5}$, and $Re_g = Du_*/\nu$; τ_c is the critical shear stress for entrainment obtained from the Inman curve [*Miller et al.*, 1977].

Southard and Boguchwal [1990] [see *Venditti*, 2003], although all the bed forms developed were 3-D. Bed forms developed instantaneously from a flat sand bed at flows A, B and C, while at flows D and E, bed forms were initiated from artificial defects placed on the otherwise flat bed. Discharge during the lowest flow stage (E) was increased from 0.0546 m^3 s^{-1} to 0.0759 m^3 s^{-1} (the highest flow, A) after 12 hours to observe the effect of a flow change on bed state. The high-flow portion, referred to as flow E_A, was also 12 hours.

[8] Bed surface topography was digitized using two acoustic echo sounders built by the National Center for Physical Acoustics (NCPA) at the University of Mississippi. The sensors had a nominal resolution that was much greater than the grain size in the experiments, which was their practical resolution. The sensors were mounted in the center of the channel with a streamwise separation of 0.133 m at ~10.50 m from the head box. Instrument signals were sampled 60,000 times at 4 Hz providing 3 to 4 hour time series of changes in bed topography.

[9] Bed load transport measurements were taken at each flow strength using a miniaturized Helley-Smith sampler with a 50 × 50 mm mouth. The body of the sampler was scaled to the mouth. At the beginning of the experiments, samples of flat bed transport were taken. As bed forms developed, samples were taken as single sand waves traveled into the sampler mouth. When the bed forms became too large to sample entirely, samples were taken over the crest, stoss slope, and trough of the bed forms. Most samples over the crest and stoss regions consisted of minor bed forms that traveled into the sampler mouth as they moved over larger primary bed forms. The sampler destroyed most of the bed forms on which it was situated, so the next sample that could be taken was over the next bed form. Thus samples were infrequent in some sections of the records. Figure 1 shows that the grain size distributions of 109 bed load samples taken during the flume runs are identical to the bulk grain size distributions. All sediment sizes in the flume were mobile during the experiments.

[10] The sand bed was monitored using a high-resolution (S-VHS) video camera mounted above the flume and centered at ~10.3 m from the head box. The video was focused to capture an area 1 m^2 but the length of the flume captured was 1.33 times the width. The video was illuminated with four 100-W floodlights mounted on the flume sidewalls and oriented to intersect at the camera focal point. The side lighting produced a glare-free image with light shadows that highlighted millimeter-scale changes in the bed structure. The video records were subsampled from the tapes using a frame grabber at intervals that ranged between 1 and 10 s. These images were further analyzed to determine morphologic changes in the sand bed over time.

3. Observed Waveforms

[11] Examination of the echo-sounding records revealed three basic waveforms: long-wavelength bed undulations (Figure 2a), dunes (Figure 2b), and the features that we call sand sheets (Figure 2c). The long-wavelength undulations have periods of 2 to 3 hours (although shorter periods are observed) and vertical relief of 0.08 to 0.10 m. These waveforms move through the system slowly and likely are bars [see *Bennett and Bridge*, 1995]. They are more prevalent at higher-flow stages (flows A and B) and are nearly absent at lower flow stages (flows C, D, and E), appearing only after several hours. The forms reappeared when the flow strength was increased from E to E_A. Only a few observations of these waveforms were made per run, preventing a more detailed discussion of their characteristics. Data are more readily available on the characteristics of the dunes and the sand sheets superimposed upon them.

[12] To examine the dunes, bed height time series were plotted to highlight each bed form as in Figure 2b. The time series were decomposed by identifying several bed form features and acquiring a time t and bed height z for each point. The features included (1) bed form trough *Tr* and the point with the minimum height z_{min} in the lee of the bed form; (2) slip face base *SFB* and slip face crest *SFC*, which are the lowest and highest points bounding the bed form slip face; (3) bed form crest *C* and the local maximum height z_{max} on the bed form; (4) a first stoss surface slope break *B*1 that commonly defined the downstream extent of the upstream dune trough; and (5) a second stoss surface slope break *B*2 that commonly occurred between the first slope break and the z_{min} of the upstreambed form. Points were often combined on bed forms (i.e., *SFB* often coincided with *Tr* and *SFC* often coincided with *C*). Stoss surface

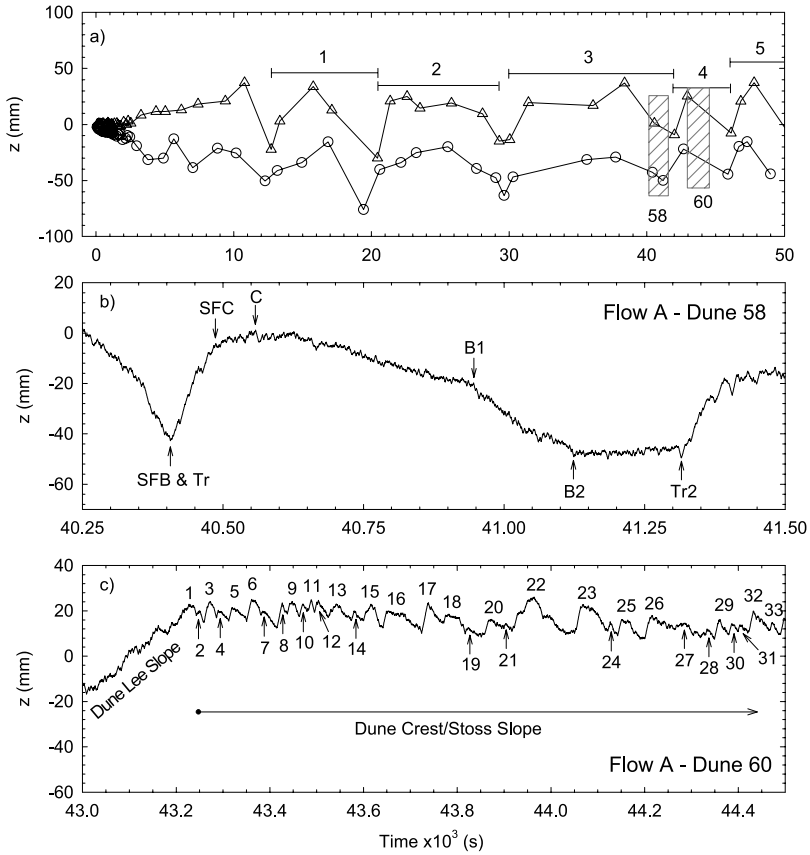

Figure 2. Examples of the waveforms observed in the experiments, including (a) long-wavelength bed undulations, (b) dunes, and (c) sand sheets. *Tr* is the dune trough, *SFB* and *SFC* are the slip face base and crest, *C* is the dune crest, *B*1 and *B*2 are slope breaks, and *Tr*2 is the upstream dune trough. Figures 2b and 2c are subsets of Figure 2a and are indicated by the gray hatch marks. Flow over these forms was right to left.

slope breaks were observed on many bed forms but were absent on others.

[13] The sand sheets migrated over the stoss surface of the primary dune forms (usually between *B*1 and *SFC*) at rates much larger than the dune migration rate. The bed height time series were plotted to highlight the dune stoss slope and hence groups of sand sheets as in Figure 2c. The time series were then decomposed to identify t and z of the sand sheet trough and crest. These smaller bed forms were far too small and numerous to identify other feature points, although many larger sheets display these features. The morphologic characteristics and sediment transport rates associated with these forms are discussed in more detail below.

4. Dune Morphology and Scaling

[14] The development of dune length L and height H at each flow strength is shown in Figure 3. Dune height was calculated as $H = z_{max} - z_{min}$ for each echo sounder time series, providing two separate H values. Dune wavelength was calculated by (1) determining a time lag t_{lag} between the arrival of the dune *SFB* at echo sounders 1 and 2, (2) determining the time it took for a bed form to pass one of the echo sounders t_{pass}, (3) computing a dune migration rate $R = 0.133$ m/t_{lag}, and (4) computing the wavelength $L = R \cdot t_{pass}$. Since each echo sounder provided a t_{pass} value, a common R value produced two estimates of L for each bed form.

[15] Bed form growth between the sensors produces some uncertainty in the length estimates. Spatially averaged crest migration rates measured from the video at the largest two flow strengths (with the smallest morphologic change timescales) showed a decrease from ~1.5 to 0.6 mm s^{-1} during the first 2000 s, followed by a decrease of ~0.2 mm s^{-1} over the next 6000 s of the experiments [*Venditti*, 2003]. Corresponding spatially averaged lengths from the video showed a steady increase of ~0.06 mm s^{-1} during the first 5000 s of the experiment. The maximum possible increase in the bed form length (0.06 mm s^{-1} × t_{pass}) between sensors occurred during the first 2000 s and was ~7 to 11%. This maximum possible increase dropped to 4 to 5% over the next 6000 s. Typically, the increase was 1 to 2% during this period and less for the lower flow strengths. Here, we focus on bed forms that are fully developed (after 5000 s), hence the uncertainty in lengths is negligible.

[16] Uncertainty can also arise because of bed form change between the sensors. Our observations from the video indicate that fully developed dunes change little in the time required to pass through the video view, migrating at a rate of ~0.2 mm s^{-1}. This indicates that the timescale of change for the bed forms is >100 minutes, which is much longer than most t_{pass} values.

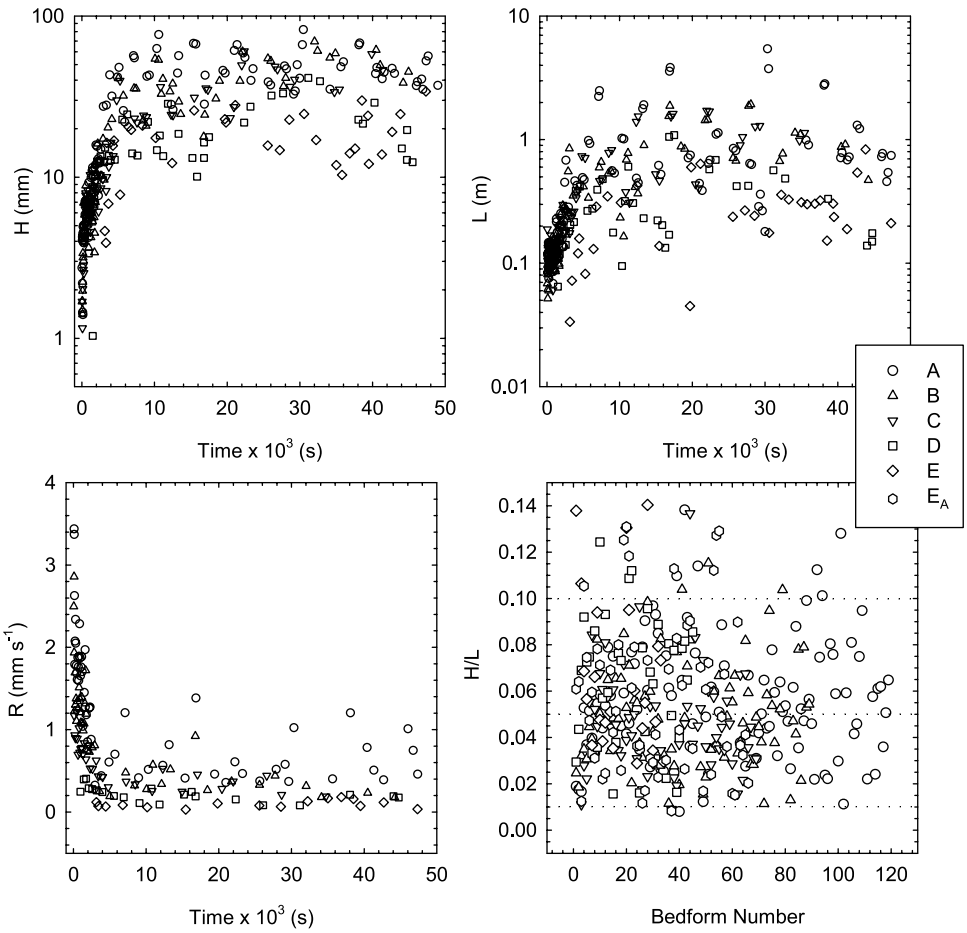

Figure 3. Dune growth curves for height H, length L, and migration rate R for flows A through E and bed form aspect ratio H/L, plotted as a function of bed form number, for flows A through E_A.

[17] During flows A, B, and C, initial dune heights H_i varied between 1.7 and 2.5 mm and initial dune length L_i varied between 0.084 and 0.105 m (Table 3). There appears to be no relation between $\overline{U}$ and H_i or L_i. Video records show a statistically significant increase in L_i with $\overline{U}$ [*Venditti et al.*, 2005], however the flows were sufficiently similar that generalizations about this relation may be unwarranted. Flow C, which did not follow this pattern in the echo sounder data, developed bed forms over the entire bed shortly after the desired flow strength was reached. However, the first bed form observation occurred several minutes into the run, which presumably bolstered L_i. Significant bed form development occurred in flows D and E as the bed forms migrated from where they were initiated to the echo sounders. Further discussion of these initial bed form characteristics can be found in work by *Venditti et al.* [2005].

[18] Once established, the dune bed forms grew in H and L while R decreased toward equilibrium values. Direct observations and subsequent examination of video suggest that the dunes underwent continuous growth in H and L rather than by capturing smaller bed forms to form larger bed forms [e.g., *Leeder*, 1980; *Raudkivi and Witte*, 1990; *Coleman and Melville*, 1994]. This process must entail a slow stretching of the bed form field by a subtle downstream acceleration of bed forms during the growth phase to accommodate the temporal deceleration.

[19] Equilibrium values of H_e, L_e and R_e (denoted by subscript e) were reached after ~1.5 hours regardless of flow strength, but all three parameters are strongly dependent on $\overline{U}$, increasing with flow strength. The similarity in the time to reach equilibrium bed form size is probably related to the limited range of flows studied in the present experiments. At flow E_A, dune heights, lengths and migration rates were similar to those observed at flow A, but no consistent pattern or equilibrium was observed. E_A bed form

Table 3. Initial and Equilibrium Dune Dimensions

Flow	H_i,[a,b] mm	L_i,[b] m	t_i, s	$\overline{H}_e$, mm	$\overline{L}_e$, m	$\overline{R}_e$, 10^{-2} m s^{-1}
A	2.47	0.0946	instant	47.70	1.172	0.0650
B	1.70	0.0842	instant	41.61	0.860	0.0371
C	1.91	0.1046	instant	35.88	0.954	0.0334
D[c]	2.35	0.0646	963	21.52	0.383	0.0172
E[c]	4.27	0.0336	3149	19.67	0.300	0.0097
E_A	NA[d]	NA	NA	NA	NA	NA

[a]Value is the average of observed height at both of the inline echo sounders.

[b]At flows A and B, values are averages of all bed forms observed during the first 3 min. At flows C, D, and E, values are for the first bed form observed.

[c]Initial measurements were taken 1.22 m downstream from where the bed forms were initiated.

[d]NA is not applicable.

lengths and heights continued to increase after 12 hours, and thus were not in statistical equilibrium at the end of the run. Since the experimental run-time periods of E and E_A were the same, it is safe to conclude that the time to reach statistical equilibrium is longer when bed forms must adjust to a new hydraulic condition as compared to when they develop from a flat bed. The time to equilibrium is not independent of initial conditions. Bed morphology adjustment lagging behind changes in bulk hydraulics has been observed frequently in large rivers [cf. *Pretious and Blench*, 1951; *Allen*, 1973; *Villard and Church*, 2003] and has previously been observed in flume experiments (at a scale similar to those presented here) where adjustment to new flow conditions required several days (R. Kuhnle, personal communication, 1999). It is likely that the bed form properties observed at flow E_A and the associated sediment transport rate are reflections of an ongoing adjustment to the new hydraulic conditions.

[20] *Yalin* [1964] suggests that dune dimensions should scale as $H = d/6$ and $L = 5d$ but these relations vary with excess shear stress [*Bridge*, 2003], changing dramatically when the suspension threshold is exceeded [*Fredsoe*, 1982]. In this context, *Allen* [1982] suggests rather wide ranges for the depth scaling $d/2.5 < H < d/40$ and $d < L < 16d$. Observations here fall within Allen's wide ranges but are similar to Yalin's original depth scalings. *van Rijn* [1984] casts bed form height in terms of an excess shear stress (referred to as a transport stage) and our observations compare well with empirical relations proposed for dunes. The observed variation in H_e and L_e with $\overline{U}$ for a given flow depth is likely a reflection of the scaling of bed form size with excess shear stress.

[21] A coherent scaling for bed form migration rate has not been presented in the literature, but there are a number of empirical relations linking R to velocity head ($\overline{U}^2/gd$) (Pushkarev (1936), as discussed by *Yalin* [1977]), D and viscosity [*Kudrjashev*, 1959], Re_g [*Thomas*, 1967], and excess shear stress [*Coleman and Melville*, 1994], yet there are serious problems with each. Pushkarev derives a relation by plotting $\overline{U}^2/gd$ on both axes causing an unknown level of autocorrelation. *Kudrjashev*'s [1959] relation was derived for coarse sand and fine gravel (D = 1 to 3 mm). *Thomas*'s [1967] relation contains an empirical coefficient related to slope whose variation is not known. *Coleman and Melville*'s [1994] relation was derived using data from a narrow flume where extensive bed form coalescing was observed as the growth mechanism (this was not observed as the growth mechanism in the much wider flume used in our experiments and the impact of this difference cannot be assessed). Nevertheless, the *Kudrjashev* [1959] and *Coleman and Melville* [1994] relations predict R values to within an order of magnitude of those observed here.

[22] According to classifications presented in Table 1, use of the term dune for the relatively larger-scale bed form appears justified. The sediment D_{50} is near the upper limit expected for ripples to form. Flows are not hydraulically smooth (Table 2). We have only a few observations of bed forms with aspect ratios <0.01, the usual lower limit of dunes, while 49% of aspect ratios are <0.05, the typical lower limit of ripples. Equilibrium lengths at flows A, B and C exceed the grain size scaling typical of ripples $L = 1000D$ [*Yalin*, 1964], although L_e does fall within this range at flows D and E. The excess shear stress in the experiments (Table 2) is capable of creating ripple features, but not at D = 0.5 mm. The features plot in the dune field of the bed form existence diagrams of *Southard and Boguchwal* [1990] although flow E plots at the boundary between ripples and dunes [see *Venditti*, 2003]. There was no systematic change in the bed form aspect ratio with time, implying that the small-scale forms that arose on the flat bed at the beginning of the runs were dunes that grew and not ripples that later evolved into dunes.

5. Sand Sheet Morphology and Scaling

[23] Sand sheets migrating over the dune backs were examined using both the video records and the decomposed echo sounder time series, which were employed to determine the sand sheet height H_{ss} and frequency f_{ss}. The method used to determine dune R and L could not be applied to determine the sand sheet migration rate R_{ss} and length L_{ss} because the small bed forms were moving quickly enough that more than one sheet could pass echo sounder 1 before being sensed by echo sounder 2.

[24] To overcome this problem, the video records taken at flow strength B were used to determine sheet R_{ss} and L_{ss}. Nine sections of video taken during flow B were chosen for detailed analysis of the sand sheets over five separate dunes at experimental times of ~2, 3.5, 5.2, 8 and 11.7 hours. Four sections of video were chosen over one dune to determine the consistency of measurements of sand sheets on an individual dune, as it evolved. Once sections of video were chosen, five successive images were drawn from the video, each separated from the next by 10 s. The dune crests and sheet crests were digitized from each image using GIS software. By overlaying the sheet crests from successive images, the horizontal distance traveled by the sheet crests could be measured (Figure 4). Horizontal lines separated by 0.05 m vertically from top to bottom were overlaid on the image and horizontal distances were measured, including L_{ss} and the migration distance between subsequent images. L_{ss} is defined as the length between two crests, so we cannot define the length of the most upstream sheet on the dune back. Dividing the migration distance by the separation time between the images, the migration rate R_{ss} can be estimated. Dune length was determined by measuring the areal extent of the dune and dividing by its cross-stream extent, which was measured from the same video image.

5.1. Sand Sheet Characteristics From Video

[25] Sand sheet lengths measured from the video were all approximately the same (see Figure 4), implying there was no change in L_{ss} with distance along the dune. Further, L_{ss} averaged for individual measurement sets did not display any relation to L (Figure 5). Mean L_{ss} is unchanged across a range of R values. Hence L_{ss} is invariant with dune size. On the basis of the similarity in sheet lengths, measurements can be aggregated (Figure 5). Lengths generally varied between 0.02 and 0.28 m and had a mode of 0.10 to 0.12 m.

[26] The sand sheet migration rate does not appear to increase with distance along the dune (see Figure 4) indicating that the sheets are not accelerating up the stoss slope of dunes. In contrast to L_{ss}, R_{ss} does vary with dune size, roughly decreasing with L and, in accordance with

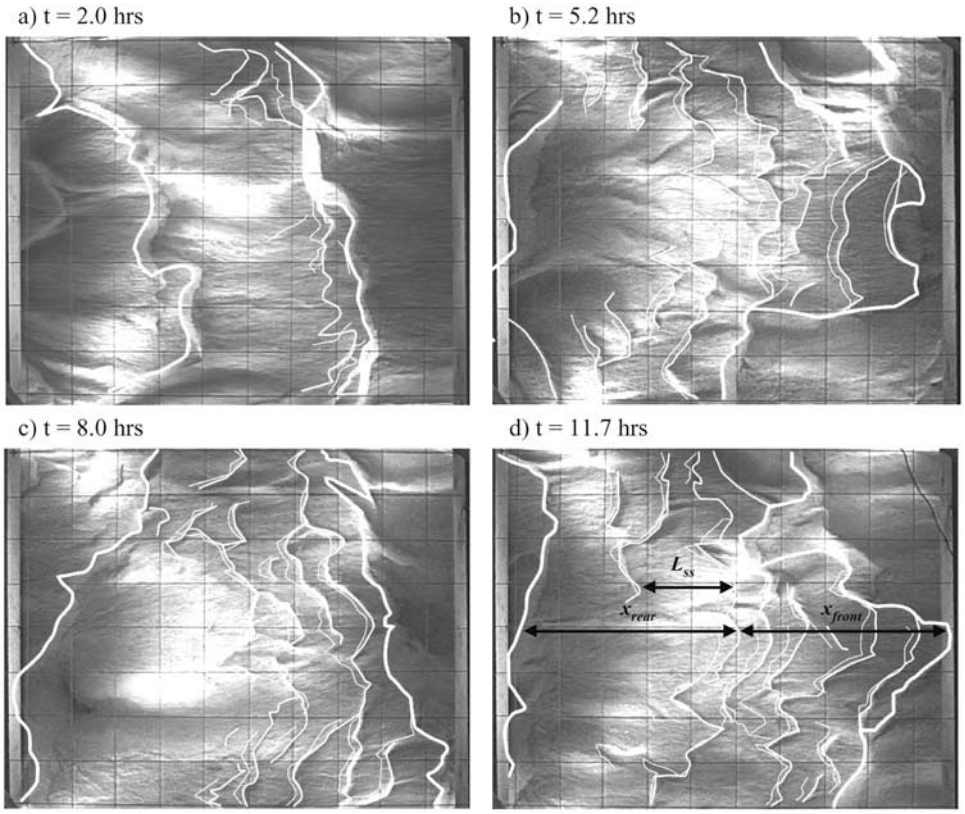

Figure 4. Examples of the video images grabbed from the overhead video camera. All images were taken during flow B. Lines indicate the features digitized from the image, including dune crest lines (thick white lines), sand sheet crest lines from the current image (medium white lines), and sand sheet crest lines from the image taken 10 s prior (thin white lines). Measurements were made along 20 horizontal transects of sand sheet lengths L_{ss}, migration distances between paired images, distance from the upstream dune crest line to the first sand sheet crest line x_{rear}, and distance from the first sand sheet crest line to the downstream dune crest line x_{front}. Grid spacing is 0.115 m, and flow is left to right.

visual observations, it roughly increases with R (Figure 5). For seven of the nine measurement sets, R_{ss}/R = 8 to 10 while two points had a ratio of 6. We consider these two points to be outliers. This likely occurred because the primary fluid vector deviated from the sheet migration vector, reducing the sheet migration rate in the streamwise direction. The primary fluid vector was observed to vary substantially and is ultimately controlled by upstream bed form shapes and orientations. Including these points in a regression through the points in Figure 5 does not significantly alter the relation since we set the origin to as the intercept (when $R_{ss} = 0$, $R = 0$). If the points are not included the relation, R_{ss}/R = 9.2 and if included, R_{ss}/R = 8.0. Aggregated R_{ss} ranged between 0.2 and 5 mm s^{-1} with a mode at ~2 mm s^{-1} (Figure 5).

5.2. Sand Sheet Characteristics From Echo Sounders

[27] Sand sheet heights plotted relative to position along the bed form are displayed in Figure 6a, and mean heights averaged over each dune are displayed in Figure 6b. The majority of sand sheet heights varied between 1 and 20 mm (i.e., 2 to 40 D), although some H_{ss} values fell outside this range over the largest dunes. Larger sheets tend to be near the dune crest (Figure 6a), but this does not translate into H_{ss} consistently increasing toward the dune crests. Although sand sheet sequences could be identified in which H_{ss} increased toward the crest, many dunes exhibited random sequences of H_{ss} (no pattern) toward the crest, and many others displayed nearly constant values of H_{ss} [see *Venditti*, 2003].

[28] Mean sheet height $\overline{H}_{ss}$ increased during the experimental run in the same fashion as H and L, increasing dramatically until an equilibrium was established (Figure 6b). Unlike sheet length, $\overline{H}_{ss}$ increased with bed form size. In fact, the normalized sand sheet height H_{ss}/H is centered at or near 0.1 for all flow strengths (Figure 6c). Normalized sheet height generally varied between 0.02 and 0.30, although distributions are skewed toward lower values.

[29] The frequency of sand sheet passage over the back of a dune is the number of crests observed n divided by the period of time that sheets are passing the probe t_{tot}, expressed as $f_{ss} = n/t_{tot}$. Sand sheet frequencies range between 0.01 and 0.15 Hz and, with the exception of sheets at flows E and E_A, appear to fall into two groups (Figure 6d). Over the incipient dunes at the beginning of the runs, many f_{ss} values are rather large with more than 8 sheets advecting past the echo sounders per 100 s. The averages varied between 12 and 16 sheets/100 s. In contrast, over the larger dunes later in the runs, generally fewer than 8 sheets/100 s were observed and, on average, 3 to 4 sheets/100 s. The

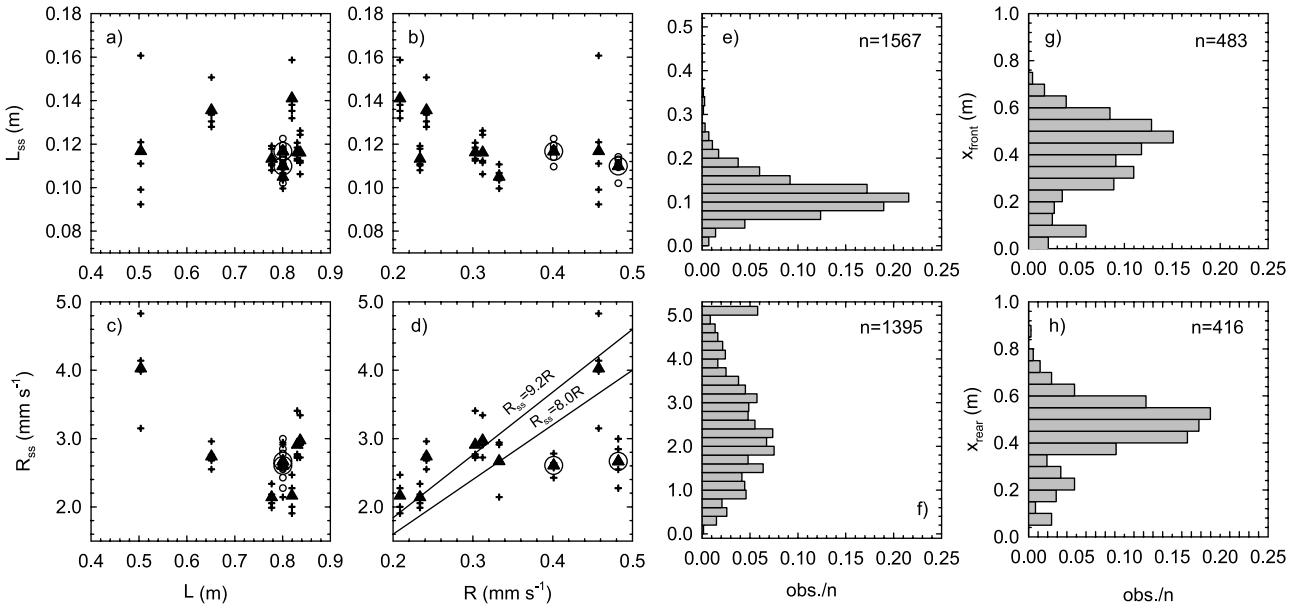

Figure 5. Sand sheet properties measured from the video. (a, b, c, and d) Sand sheet lengths L_{ss} and migration rates R_{ss} plotted against dune lengths L and migration rates R as measured from the video. Aggregate sand sheet properties measured from the video: (e) lengths L_{ss}, (f) migration rates R_{ss}, (g) distance from the first sand sheet crest to the major bed form crest x_{front}, and (h) distance from the rear bed form crest to the first sand sheet crest x_{rear}. In Figures 5a–5d, open circles are the image averages, and triangles are averages for each dune. The regression line labeled $R_{ss} = 9.2R$ excludes the circled triangles, and the line labeled $R_{ss} = 8.0R$ includes these points.

larger values of f_{ss} all occurred over rapidly growing and somewhat diminutive dunes.

[30] At flow strength E the higher grouping is not apparent; nearly all f_{ss} values were below 8 sheets/100 s. These dunes had comparatively little sediment moving over the stoss slope and there may have been insufficient amounts of sand to produce sheets. Yet, many of the larger bed forms were superimposed by sheets. When the flow was increased to flow strength E_A, the bed already had well developed dunes, and thus differed from other runs in which the dunes with large f_{ss} values were still quite small in size. When the dunes were most unstable (i.e., at the flow change), f_{ss} exceeded 8 sheets/100 s.

[31] Sand sheet lengths were estimated from the echo sounders using the video analysis results by (1) determining an approximate value of R_{ss} for each dune from the regression between R_{ss} and R (Figure 5) and (2) finding the time that each sheet required to pass the sensor (t_{pass}). Sand sheet length was calculated as $L_{ss} = R_{ss} \times t_{pass}$. This method explicitly assumes that the $R_{ss} - R$ relation derived for flow B holds for the other flows (A, C, D, E) we observed in our experiments. Fortunately, the range in flows is quite small and the form of the relation is intuitively correct; an increase in the migration rate of bed forms superimposed on the dune back delivers more sediment to the bed form slip face, increasing its forward rate of advance. Sand sheet lengths, plotted relative to position along the bed form, are displayed in Figure 6e and mean lengths, averaged over each dune, are displayed in Figure 6f. There was a propensity to observe large sheet lengths near the crest but, like patterns observed for H_{ss}, there were no consistent patterns in L_{ss}. Sheet lengths generally varied between a few centimeters and 0.5 m. The sheet lengths are generally less than 0.3 m (Figure 6g), and the distribution tends to be strongly skewed toward smaller lengths with the mode between 0.04 and 0.06 m. Mean sheet length $\overline{L}_{ss}$ varied between 0.05 and 0.40 m at the larger flow strengths (A, B, and E_A) while, at the lower flow strengths (C, D and E), $\overline{L}_{ss}$ varied between 0.02 and 0.2 m (Figure 6f). The clear initial increase in $\overline{H}_{ss}$ is not observed for sheet length.

6. Discussion

[32] The recognition of migrating sand sheets on dune stoss sides raises questions about their classification, scaling and origin, as well as their impact on total bed load flux on a dune-covered bed. More generally, their role in relation to bed deformation and the development of the dunes requires elucidation.

6.1. Sand Sheet Classification and Scaling

[33] Sand sheets cannot be classified easily as ripples or dunes, though they have characteristics shared with both features. Ripples can form in 0.5 mm sand, although sediment of this size is near their expected grain size limit (see Table 1). The relatively small lengths and heights of sand sheets are reasonable for ripples [cf. *Ashley*, 1990]. Sand sheets were not observed to grow as they migrated downstream, suggesting that they are not growing to scale with a characteristic depth scale such as the internal boundary layer and, further, that when sand sheets appear on the dune stoss slope, they are at their equilibrium dimensions. This behavior is typical of ripple features that scale with grain size, but the lifespan of the observed features was insufficient to assess these appearances properly. In any case, some authors argue that ripples grow from smaller

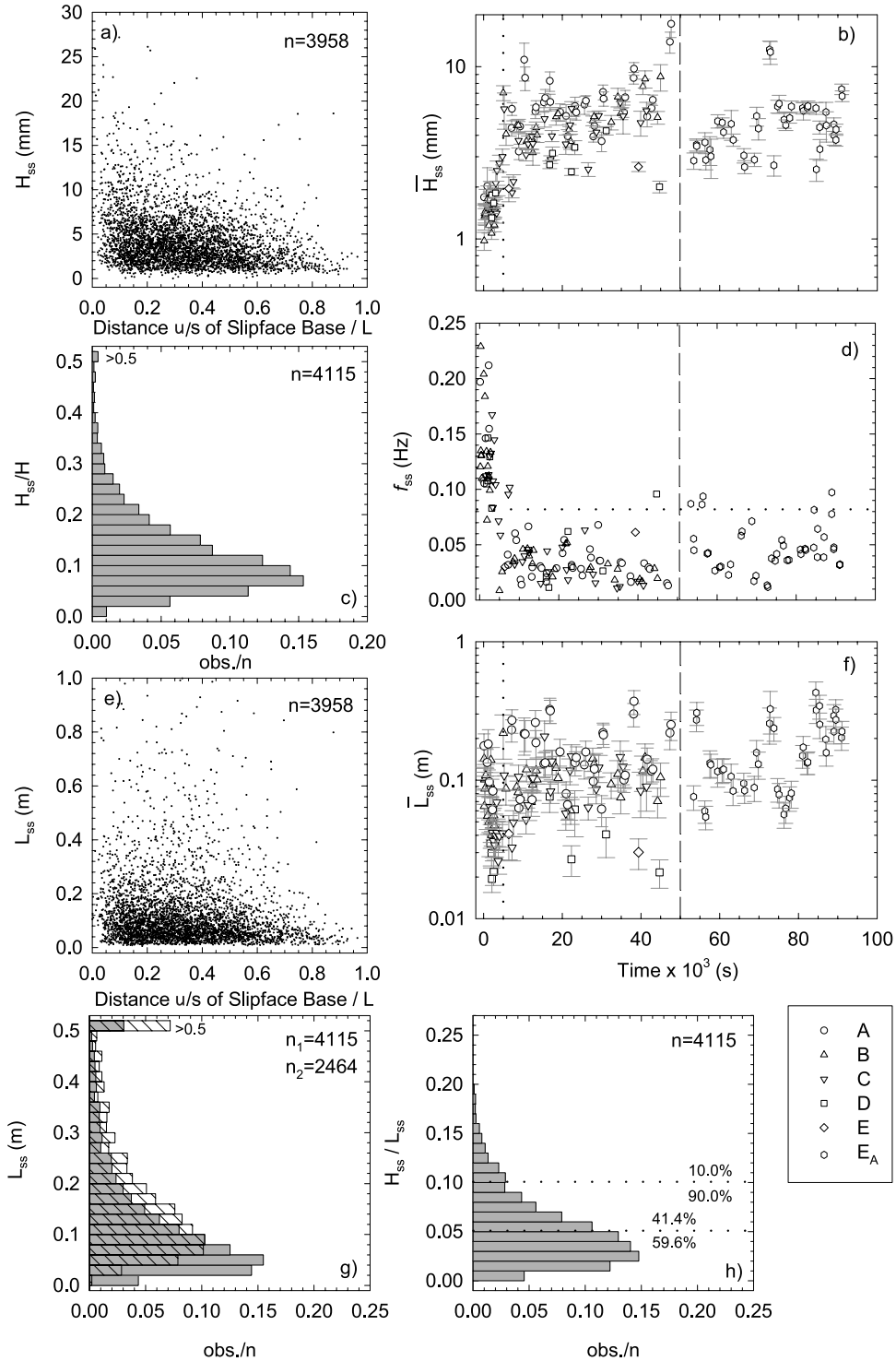

Figure 6

nascent bed waves [cf. *Coleman and Melville*, 1996; *Raudkivi*, 1997]. Sand sheets are much smaller than the ripple scaling suggested by *Yalin* [1964, 1985], and none of the flows were hydraulically smooth. The excess shear stress is within the ripple range proposed by *van Rijn* [1984] (Table 2), but the grain size exceeds *van Rijn*'s [1984] suggested limit for ripples (0.45 mm; see Table 1). It must be recognized, however, that the grain Reynolds number and excess shear stress values are based on bulk hydraulic values; local values on the dune backs may not be adequately reflected in these parameters.

[34] Sand sheets tend to have aspect ratios far smaller than observed for ripples but within the range expressed by dunes. Figure 6h shows histograms of the sand sheet aspect ratio (H_{ss}/L_{ss}). On the basis of the separation between ripples and dunes given by *Allen* [1968], some of the sand sheets could be ripple forms, but most sheet aspect ratios fall below the upper limit for dunes (0.1). Further, at flow strengths A,

B, C, and E_A, more than 55% of the sheets have aspect ratios smaller than the lower limit for ripples (0.05, suggested by *Guy et al.* [1966] and *Allen* [1968]). Even at flow strength D, 36% of the sheets have aspect ratios smaller than 0.05. Distributions of H_{ss} and L_{ss} are not well defined at flow E because only two bed forms were observed with superimposed sheets. Modal aspect ratios for other runs lie between 0.02 and 0.05, depending on the run. These aspect ratios suggest that sand sheets are not ripples but low-relief dunes. Yet, depth scaling is not observed. It remains possible that, if the dunes were longer, sheet growth might occur to result in scaling with the internal boundary layer thickness.

[35] Sand sheets share several morphological characteristics with bed load sheets. Bed load sheets are typically several coarse grain sizes high, lack a well-defined slip face, and have aspect ratios between 0.003 and 0.040, which classify them as low-relief dunes [*Bennett and Bridge*, 1995]. It is generally agreed that bed load sheets are caused by selective entrainment and transport in heterogeneous sediment [*Whiting et al.*, 1988; *Bennett and Bridge*, 1995]. Direct observations and subsequent examination of side view video suggest many sand sheets did not have a conventional slip face composed of sand grains avalanching down a slope near the angle of repose. Instead many sheets appeared to be simple advecting waves. At 0.1 H and with lengths that range from a few centimeters to ~0.3 m, H_{ss} and L_{ss} are similar to bed load sheet heights and lengths observed over dunes [e.g., *Whiting et al.*, 1988; *Livesey et al.*, 1998]. However, simply analogizing the sand sheets with the bed load sheets previously described seems inappropriate because they cannot be attributed to selective entrainment and transport. No sediment sorting can occur since the sand is homogeneous (Figure 1). Furthermore, the height of the sand sheets is not limited to a few grains. Sand sheets may be a species of bed load sheet developed in the regime of full bed material mobility where the features develop relative heights of order 10 to 100D because of the much smaller grain size and relative roughness. Interestingly, both *Whiting et al.* [1988] and *Seminara et al.* [1996], in a theoretical analysis of bed load sheet stability, remark on the dune-like properties of bed load sheets.

[36] That the sheets cannot be readily classified highlights a general problem in the literature. The available classifications contain overlaps in criteria and conflict in interpretation and application. Until ripples and dunes formed in unidirectional flow are demonstrated to be formed by different mechanisms or their properties controlled by different hydrodynamic processes, the division of ripples from dunes by other means will remain an artificial separation of genetically related features [*Rubin and McCulloch*, 1980].

6.2. Origin of Sand Sheets

[37] Development of the sand sheets appears to be related to a minimum distance beyond the bed form crest over which the sediments that will form the sheets are entrained and accumulated. This is revealed in measurements from the video of the distance from the upstream dune crest to the first observed sand sheet crest x_{rear} and the distance from the downstream dune crest to the first observed sand sheet crest x_{front} (see Figure 5). Most x_{rear} values are between 0.35 and 0.60 m, while x_{front} varied with L. Thus proximity to the dune crest does not appear to be an important factor but a minimum x_{rear} value of ~0.5 m is necessary for the sheets to form. This appearance is further substantiated by the fact that no sheets appeared in the video until the bed forms reached a wavelength of ~0.5 m.

[38] The sheets appear to form downstream of the reattachment point x_R. Assuming $x_R \approx 5\ H$ [cf. *Engel*, 1981], the separation cell would sit at approximately $0.8 < x/L < 1.0$ over most of the bed forms. Echo soundings indicate that sand sheets generally do not form upstream of $x/L = 0.8$ (see Figures 4, 6a, and 6e). Interestingly, x_{rear} is not a consistent distance downstream of x_R. When $L = 0.5 - 1$ m, $x_{rear} \approx 3\ x_R$, but $x_{rear} \approx 2\ x_R$ when the bed forms are larger. Thus where the sand sheets appear on the dune back does not scale with x_R over the smaller dunes nor do they form a consistent distance downstream of x_R.

[39] The sand sheets migrating over dunes are similar to those developed at the beginning of the experimental runs over the flat bed [*Venditti et al.*, 2005], although they have less regular crest line shapes. Near-bed flow velocities and bed form scales are similar over the dunes and the flat bed suggesting it is possible that the same processes that control sand wave initiation and development over a flat bed may be operating here [see *Venditti et al.*, 2005].

Figure 6. Characteristics of sand sheets. (a) Sand sheet height H_{ss} plotted against the distance upstream of *SFB* normalized by the dune length. (b) Mean sand sheet height $\overline{H}_{ss}$ plotted against run time. (c) Histograms of H_{ss} normalized by dune height H. (d) Mean sand sheet frequency f_{ss} plotted against run time. (e) Sand sheet length L_{ss} plotted against the distance upstream of *SFB* normalized by the dune length. (f) Mean sand sheet length $\overline{L}_{ss}$ plotted against run time. (g) Histograms of L_{ss} calculated using the relation between R_{ss} and R. The solid bars are for all lengths measured from the echo sounders. There is an evident difference between this length distribution and the one in Figure 5e because the resolution of sheet height using the echo sounders is much greater than the resolution of sheet length from the video. Thus we can see sheets with smaller associated lengths from the echo sounders. The observations differ between the two approaches because the thresholds are different. Removing sand sheet lengths that would not be visible in the video (where $H_{ss} < 3$ mm), excessively long sheets that were generally ignored in the video (where $L_{ss} > 0.5$ m), and sheets over small bed forms where the frequency was large ($f_{ss} > 0.08$ Hz) (hatched bars) substantially improves the comparison. The numbers of observations for the unfiltered data n_1 and filtered data n_2 are indicated. (h) Histograms of sand sheet aspect ratio H_{ss}/L_{ss}. The dotted line at 0.10 indicates the typical upper limit of dunes, and the dotted line at 0.05 indicates the usual lower limit of ripples. In Figures 6b, 6d, and 6f, averages are for individual dunes. In Figures 6b and 6f, error bars are the standard error ($\pm\sigma/\sqrt{n}$). Equilibrium dune size occurs at ~5000 s during each run (dotted vertical line) (Figure 3). All runs end at ~12 hours (vertical dashed line in Figures 6b, 6d, and 6f), with the exception of flow E, which was adjusted to a higher flow strength E_A.

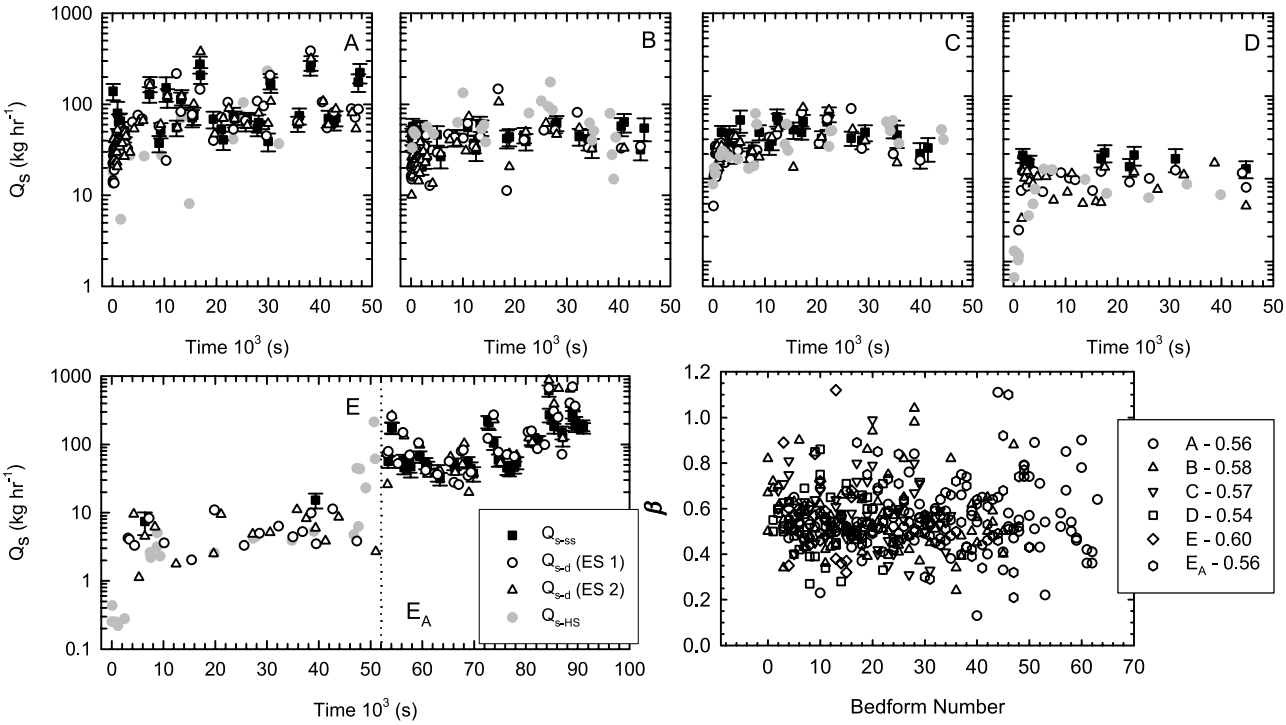

Figure 7. Sediment transport rates Q_S determined from the morphologic characteristics of the dunes Q_{s-d} (ES 1 and ES 2 refer to echo sounders 1 and 2), the morphologic characteristics of the sand wave sheets Q_{s-ss}, and Helley-Smith bed load samples Q_{s-HS}. Sand sheet error bars are calculated by combining the standard error ($2\sigma/\sqrt{n}$) for H_{ss} and the error from the regression line between R and R_{ss} using rules for combining error from multiple measured quantities [*Beers*, 1957]. Figures 7a–7e show results from experiments A–E. Also plotted is the bed form shape factor β.

6.3. Sediment Transport Rates

[40] Although bed load transport measurements were made during the experiments, they were too infrequent to provide a complete picture of the sand transport associated with the waveforms. Nearly all the bed material was transported as bed load; sand suspension and sand bypassing bed forms as it traveled downstream were observed to be negligible. Thus more complete quantification of the transport can be accomplished by using morphological estimates based on the characteristics of the waveforms themselves.

[41] *Simons et al.* [1965] indicate the volumetric dry sediment transport rate of bed forms moving at a migration rate R_b per unit time and unit width is

$$Q_s = \beta(1 - P)R_b\, h \tag{1}$$

where P is the sediment porosity (~0.4 for 0.5 mm sand [*van Rijn*, 1993]) and β is the bed form shape factor, determined from $\beta = A/hl$ (A is the cross-sectional area of the bed form). The echo sounder time series were used to calculate β for the dunes by defining A from features shown in Figure 2 (i.e., *Tr*, *SFB*, *SFC*, *C*, *B*1, and *B*2) and a datum line running between *Tr* and the upstream *Tr*. Values of β ranged between 0.3 and 0.8 with greater variance later in the runs. For all runs, mean β is ~0.56 (Figure 7), similar to values previously reported [cf. *van den Berg*, 1987; *ten Brinke et al.*, 1999].

[42] It can be argued that equation (1) is biased because the entire bed form is not partaking in transport [cf. *Engel and Lau*, 1981] and that there is an upstream component of transport under the separation cell that is not considered. The former of these is incorrect. Over some timescale, the entire bed form is involved in downstream transport unless the channel is locally aggradational or there is upstream transport in the bed form trough. Upstream transport under the separation cell requires that the upstream flow be sufficiently strong to move particles and this only happens over very large bed forms or when bed forms are laterally constrained (as in a narrow flume [cf. *Allen*, 1982]). Further, the separation cell is a persistent feature of the flow field only in the time-averaged sense. Fluid composing the separation cell is frequently expunged from the lee of the bed form as part of the macroturbulence generation process [*Nezu and Nakagawa*, 1993; *Kostaschuk and Church*, 1993; *Venditti and Bennett*, 2000]. Providing sediment is not suspended in the lee of the bed form, net transport in the separation cell is negligible.

[43] Figure 7 shows sediment transport rates for dunes Q_{s-d}, sand sheets Q_{s-ss}, and Helley-Smith bed load samples Q_{s-HS}. The dune-related transport rate is estimated using $h = H$ and $R_b = R$ and the sand sheet–related transport is estimated using $h = \overline{H}_{ss}$ and $R_b = R_{ss}$ in equation (1). Sheet heights and migration rates are averaged over a dune. Since the sand sheets have approximately the same morphological scaling as the dunes, a β value of 0.56 is used for all sheets. Equation (1) assumes that the bed forms are not deforming with time. As mentioned above, the dune forms can undergo some deformation, but the time required for significant change is much longer than the observation window. Sheets can undergo deformation much more quickly, but the observation window is similarly smaller.

Table 4. Mean Sediment Transport Rates With the Standard Error ($\sigma/\sqrt{n}$) as Upper and Lower Bounds[a]

	Helley-Smith Samples			Dunes			Sand Sheets
Flow	n_i	$\overline{Q}_{si}$, kg h^{-1}	$\overline{Q}_{se}$, kg h^{-1}	n_i	$\overline{Q}_{si}$, kg h^{-1}	$\overline{Q}_{se}$, kg h^{-1}	$\overline{Q}_{se}$, kg h^{-1}
A	1	18.12	70.17 ± 18.47	21	27.69 ± 1.84	102.44 ± 7.66	111.71 ± 12.28
B	1	33.28	71.23 ± 9.76	17	20.74 ± 1.29	47.91 ± 4.83	46.47 ± 2.33
C	2	11.04 ± 2.46	35.64 ± 3.23	9	15.76 ± 2.35	34.16 ± 3.85	36.67 ± 2.66
D	6	1.50 ± 0.42	9.01 ± 1.13	0	NA	9.45 ± 0.62	17.05 ± 1.19
E	5	0.29 ± 0.04	13.67 ± 8.22	0	NA	5.66 ± 0.58	11.32 ± 3.93
E_A	NA	NA	NA	0	NA	173.47 ± 25.45	126.01 ± 16.84

[a]Subscript i indicates the initial values, and e indicates the equilibrium values (mean of estimates/measurements taken after 5000 s). Helley-Smith samples in the dune trough are removed from the averages. No Helley-Smith samples were taken at flow E_A. The initial Helley-Smith transport values are for a flat bed, a condition that existed for varying amounts of time. For flows A–E dune-related Q_{si} is the mean of values in the first 10 min of the experiment. Because the dunes at flows D and E were generated well upstream of the echo sounders, no initial dune-related transport could be detected.

[44] Both Q_{s-d} and Q_{s-HS} increased in the same fashion as dune L and H, rising asymptotically toward an equilibrium value. Values of Q_{s-ss} were generally larger than Q_{s-d} and Q_{s-HS} when the transport rate increased toward an equilibrium at flow strengths A, B, C and D. These estimates of Q_{s-ss} are derived from sand sheets with a frequency greater than 8 sheets/100 s. It appears that these sheets were moving more sand than the incipient dune forms. This is to be expected since, in order for the dune to grow, sand sheets must appropriate more sand from the dune back than moves past the dune crest.

[45] Table 4 provides the initial mean transport rates $\overline{Q}_{si}$ and the average equilibrium transport rates $\overline{Q}_{se}$ for all runs. Transport rate increases with flow strength, but $\overline{Q}_{se-d}$ at flow strength E_A, calculated over the entire 12 hour high-flow portion of the run, is larger by ~70% than at flow strength A. This again suggests that the time required for a run to reach equilibrium when bed forms are already present may be significantly longer than when they are not present.

[46] Agreement between the morphological estimates of sand transport and $\overline{Q}_{s-HS}$ is highly variable. The ratio $\overline{Q}_{si-d}/\overline{Q}_{s-HS}$ at flow strengths A, B and C are 1.53, 0.62, and 1.43, respectively. Values of $\overline{Q}_{s-HS}$ did not decrease with flow strength, which contradicts observations made during the experiments and $\overline{Q}_{si-d}$ estimates. Agreement is improved somewhat if equilibrium transport values are examined. At three of the flow strengths, $\overline{Q}_{se-HS}$ and $\overline{Q}_{se-d}$ are within 15% (Table 4). Because there are more samples during the equilibrium period of these flows, the effect of measurement error is diminished. However, it should be noted that the Helley-Smith sampler often caused significant erosion. Also, it was difficult to place the sampler flush with dune slope. Notes taken during the experiment were used to remove samples obviously in error but the results suggest that the error associated with $\overline{Q}_{s-HS}$ is still significant. Nevertheless, the Helley-Smith samples confirm that the estimates from the morphological methods are of the right magnitude.

[47] Figure 8 indicates that the correlation between Q_{s-d} and Q_{s-ss} is also variable. Transport estimates are clustered about the 1:1 line and most Q_{s-ss} estimates are within a range of 0.5 to 2× the Q_{s-d} estimate. At flow strengths A, B, and C, the ratio $\overline{Q}_{se-ss}/\overline{Q}_{se-d}$ ranged between 0.97 and 1.09 and the error bounds overlap (Table 4). At flow strength E_A, the ratio Q_{s-ss}/Q_{s-d} calculated for individual dunes averages to ~1.0 for all dunes with sand sheets, although, there appeared to be some dunes with larger transport rates that did not have superimposed sand sheets. Agreement is not as strong at flows D and E where the ratio $\overline{Q}_{se-ss}/\overline{Q}_{se-d}$ is 1.80 and 2.0, respectively. Results from flow strength E can be dismissed as the transport estimates are based on only 2 of 17 dunes and only one of those points exceeds the range of Q_{se-d}. At flow D, more sediment appears to be recruited from the dune back than is moving over the dune crest suggesting the bed forms with sheets were consistently growing. Alternatively, extrapolation of the relation between R and $R_{\min}$ derived from flow B to flows D and E may be too extreme.

[48] For sediment transport equivalence, sand sheets migrating at 10 times the dune rate must be 0.1 times the size, which is substantiated by the morphological observations. Figure 8 confirms that sediment movement over the dune back is essentially equivalent to the volume moved in the dune form. This is consistent with the contention of *Gomez and Phillips* [1999] that substantially all of the bed load in a dune field is associated with the dunes, contrary to arguments that only a portion of the dune form contributes to the transport rate [e.g., *Engel and Lau*, 1981]. Relatively large-scale wave features tend to move more slowly, while small-scale features move more quickly [cf. *Coleman and Melville*, 1994]. However, the volumetric transport rate

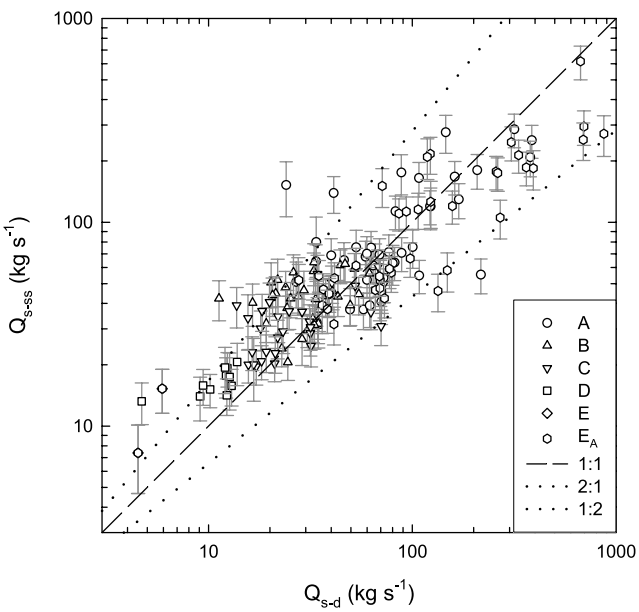

Figure 8. Correlation between the dune-related transport rate Q_{s-d} and the sand sheet–related transport rate Q_{s-ss}. Sand sheet error bars are calculated as in Figure 7.

associated with each scale is the same, suggesting that the transport rate is invariant to the scale of observation. *Raudkivi and Witte* [1990], on the basis of work by *Führböter* [1983], have suggested a coalescence of bed forms because the smaller-scale forms move faster than larger forms, which results in growth of a single bed form scale or mode. What we suggest here is that there are two separate bed form scales or modes, each in equilibrium with the imposed hydraulics, where the smaller-scale form is not causing bed form growth but is the mechanism by which material moves over the larger form producing its migration. Thus there is a cross-scale transport equivalency of two separate equilibrium bed forms. It is likely that different bed form scales typically observed in open channel flows are in sediment transport equilibrium with the flow, and that the transport associated with the larger-scale bed forms is simply the sum of all the smaller scales of transport.

7. Conclusions

[49] Observations of bed form superposition in rivers and streams are common. Yet our understanding of bed form hierarchies is incomplete, especially where multiple scales are in statistical equilibrium and simultaneously active in the channel. The kinematics and dynamics of low-amplitude, small-scale sand waves developed over migrating dunes are examined using data drawn from laboratory experiments. We refer to the small-scale superimposed sand waves as sand sheets because the features could not be classified easily as ripples, bed load sheets, or dunes. Instead the sand sheets share properties with each. The sheets have heights that are typically 0.1 times the height of the dune upon which they are superimposed, migrate at 8 to 10 times the dune rate, and have lengths that are nearly constant over the full range of dune lengths and flow conditions. Aspect ratios are generally <0.1 with a mode of ~ 0.025. The sheets form at ~ 0.5 m from the dune slip face, downstream of the reattachment point on the dune stoss slope, and this distance is invariant with dune size. Many of the sheets lack slip faces and are simple advecting waves of sediment, while others develop avalanching slopes at their head.

[50] Superimposed bed waves are often considered simply as additional roughness elements on the dune back or features formed by lag effects in environments with widely varying flows. However, our results indicate that both bed form modes (dunes and sheets) have clearly defined time and length scales. Further, total bed load flux over the dunes, and hence the migration of the entire bed form, appears to be controlled by these small-scale waveforms. The transport rate is invariant to the scale of sand wave observed. Sediment transport associated with large-scale bed forms may be simply the sum of the transport associated with the smaller-scale features.

Notation

A	bed form cross-sectional area
d	flow depth
D, D_{50}	grain size and its median
f_{ss}	frequency of sand sheet passage
ff	friction factor
Fr	Froude number
G	gravitational acceleration
h	generic bed form height
H, H_i, H_e	dune height, its initial value, and its equilibrium value
H_{ss}, $\overline{H}_{ss}$	sand sheet height and its mean value over a dune
l	generic bed form length
L, L_i, L_e	dune length, its initial value, and its equilibrium value
L_{ss}, $\overline{L}_{ss}$	sand sheet length and its mean value over a dune
n	number of observations
P	porosity of sand
Q	discharge
Q_s, Q_{si}, Q_{se}	bed load transport rate, its initial value, and its equilibrium value
Q_{s-HS}	bed load transport measured using a Helley-Smith sampler
Q_{s-d}, Q_{s-ss}	bed load transport estimated from morphology of dunes and sand sheets
R, R_e	dune migration rate and its equilibrium value
Re, Re_g	Reynolds number and grain Reynolds number
R_b	generic bed form migration rate
R_{ss}	sand sheet migration rate
S	water surface slope
t	time interval
t_{lag}	time between arrival of bed form SFB at to echo sounder 1 and 2
t_{pass}	time required for a bed form to pass one echo sounder
t_{tot}	duration sand sheets passing one echo sounder over a dune
$\overline{U}$	mean flow velocity
u_*	shear velocity
x	distance alongstream
x_{front}	distance from first sand sheet crest line to the downstream dune crest line
x_{rear}	distance from upstream dune crest line to the first sand sheet crest line
x_R	reattachment length
z, $z_{\max}$, $z_{\min}$	height about datum, its maximum value, and its minimum value
β	bed form shape factor
ν	kinematic viscosity
ρ	density
τ	boundary shear stress

[51] **Acknowledgments.** Financial support to J.V. came through a UBC University Graduate Fellowship, a Natural Science and Engineering Research Council of Canada (NSERC) postgraduate scholarship, and a research assistantship provided through a NSERC discovery grant to M.C. Funds for the experiments were provided by the U.S. Department of Agriculture and NSERC. The video image frame grabber was purchased using a Ph.D. research grant from the Association of American Geographers Geomorphology Specialty Group. N. Manklow assisted with the analysis of the echo soundings. J. Cox, J. Milam, and D. Wren at the USDA-ARS and V. Kujala at UBC provided technical support. Comments made by the journal reviewers and the associate editor were greatly appreciated.

References

Allen, J. R. L. (1968), *Current Ripples*, Elsevier, New York.

Allen, J. R. L. (1973), Phase differences between bed configuration and flow in natural environments, and their geological relevance, *Sedimentology*, *20*, 323–329.

Allen, J. R. L. (1982), *Sedimentary Structures: Their Character and Physical Basis*, Elsevier, New York.

Allen, J. R. L., and J. D. Collinson (1974), The superimposition and classification of dunes formed by unidirectional aqueous flows, *Sediment. Geol.*, *12*, 169–178.

Ashley, G. M. (1990), Classification of large-scale subaqueous bedforms: A new look at an old problem, *J. Sediment. Petrol.*, *60*, 160–172.

Beers, Y. (1957), *Introduction to the Theory of Error*, Addison-Wesley, Boston, Mass.

Bennett, S. J., and J. S. Bridge (1995), The geometry and dynamics of low-relief bed forms in heterogeneous material in a laboratory channel, and their relationship to water flow and sediment transport, *J. Sediment. Res., Sect. A*, *65*, 29–39.

Bridge, J. S. (2003), *Rivers and Floodplains*, Blackwell, Malden, Mass.

Carey, W. C., and M. D. Keller (1957), Systematic changes in the beds of alluvial rivers, *J. Hydraul. Div. Am. Soc. Civ. Eng.*, *83*, 1–24.

Coleman, J. M. (1969), Brahmaputra River: Channel processes and sedimentation, *Sediment. Geol.*, *3*, 129–239.

Coleman, S. E., and B. W. Melville (1994), Bed-form development, *J. Hydraul. Eng.*, *120*, 544–560.

Coleman, S. E., and B. W. Melville (1996), Initiation of bed forms on a flat sand bed, *J. Hydraul. Eng.*, *122*, 301–310.

Dietrich, W. E., J. W. Kirchner, H. Ikeda, and F. Iseya (1989), Sediment supply and the development of the coarse surface layer in gravel-bedded rivers, *Nature*, *340*, 215–217.

Engel, P. (1981), Length of flow separation over dunes, *J. Hydraul. Div. Am. Soc. Civ. Eng.*, *107*, 1133–1143.

Engel, P., and Y. L. Lau (1981), Bed load discharge coefficient, *J. Hydraul. Div. Am. Soc. Civ. Eng.*, *11*, 1445–1453.

Fredsoe, J. (1982), Shape and dimensions of stationary dunes in rivers, *J. Hydraul. Eng.*, *108*, 932–947.

Führböter, A. (1983), Zur Bildung von makroskopischen Ordnungsstrukturen (Stroemungsriffel und Duenen) aus sehr kleinen Zufallsstoerungen, *Mitt. Leichtweiss Inst. Tech. Univ. Braunschweig*, *79*, 1–51.

Gomez, B., and J. D. Phillips (1999), Deterministic uncertainty in bed load transport, *J. Hydraul. Eng.*, *125*, 305–308.

Guy, H. P., D. B. Simons, and E. V. Richardson (1966), Summary of alluvial channel data from flume experiments, 1956–1961, *U.S. Geol. Surv. Prof. Pap.*, *462-I*, 1–96.

Inglis, C. C. (1949), The behaviour and control of rivers and canals, *Res. Publ. 13*, vol. 2, pp. 459–465, Cent. Waterpower, Irrig. and Navig. Res. Stn., Poona, India.

Jackson, R. G. (1975), Hierarchial attributes and a unifying model of bed forms composed of cohesionless material and produced by shearing flow, *Geol. Soc. Am. Bull.*, *86*, 1523–1533.

Jackson, R. G. (1976), Large scale ripples of the lower Wabash River, *Sedimentology*, *23*, 593–623.

Kostaschuk, R. A., and M. Church (1993), Macroturbulence generated by dunes: Fraser River, Canada, *Sediment. Geol.*, *85*, 25–37.

Kudrjashev, A. S. (1959), *Alluvial Processes* (in Russian), Kondrat've, St. Petersburg, Russia.

Leeder, M. R. (1980), On the stability of lower stage plane beds and the absence of ripples in coarse sand, *J. Geol. Soc. London*, *137*, 423–429.

Liu, H.-K. (1957), Mechanics of sediment-ripple formation, *J. Hydraul. Div. Am. Soc. Civ. Eng.*, *83*, 1–23.

Livesey, J. R., S. Bennett, P. J. Ashworth, and J. L. Best (1998), Flow structure, sediment transport and bedform dynamics for a bimodal sediment mixture, in *Gravel-Bed Rivers in the Environment*, edited by P. C. Klingman et al., pp. 149–176, Water Resour. Publ., Highlands Ranch, Colo.

Miller, M. C., I. N. McCave, and P. D. Komar (1977), Threshold of sediment motion under unidirectional currents, *Sedimentology*, *24*, 507–527.

Nezu, I., and H. Nakagawa (1993), Turbulence in open channel flows, A. A. Balkema, Brookfield, Vt.

Pretious, E. S., and T. Blench (1951), Final report of special observations of bed movement in Lower Fraser River at Ladner Reach during 1950 freshet, Natl. Resour. Counc. of Can., Vancouver, B. C., Canada.

Raudkivi, A. J. (1997), Ripples on a stream bed, *J. Hydraul. Eng.*, *123*, 58–64.

Raudkivi, A. J., and H.-H. Witte (1990), Development of bed features, *Hydraul. Eng.*, *116*, 1063–1079.

Rubin, D. M., and D. S. McCulloch (1980), Single and superimposed bedforms: A synthesis of San Francisco Bay and flume observations, *Sediment. Geol.*, *26*, 207–231.

Seminara, G., M. Colombini, and G. Parker (1996), Nearly pure sorting waves and formation of bedload sheets, *J. Fluid Mech.*, *312*, 253–278.

Simons, D. B., E. V. Richardson, and C. F. Nordin (1965), Bedload equation for ripples and dunes, *U.S. Geol. Surv. Prof. Pap.*, *462-H*, 1–9.

Southard, J. B., and L. A. Boguchwal (1990), Bed configurations in steady unidirectional water flow part 2. Synthesis of flume data, *J. Sediment. Petrol.*, *60*, 658–679.

ten Brinke, W. B. M., A. W. E. Wilbers, and C. Wesseling (1999), Dune growth, decay and migration rates during a large-magnitude flood at a sand and mixed-gravel bed in the Dutch Rhine river system, in *Fluvial Sedimentology VI*, *Spec. Publ. Int. Assoc. Sedimentol.*, vol. 28, edited by N. D. Smith and J. Rogers, pp. 15–32, Blackwell Sci., Malden, Mass.

Thomas, Z. (1967), Velocity of motion of sand banks, paper presented at 12th Congress of IAHR, Int. Assoc. for Hydraul. Res., Fort Collins, Colo.

van den Berg, J. H. (1987), Bedform migration and bedload transport in some rivers and tidal environments, *Sedimentology*, *34*, 681–698.

van Rijn, L. C. (1984), Sediment transport, part III: Bed forms and alluvial roughness, *J. Hydraul. Eng.*, *110*, 1733–1754.

van Rijn, L. C. (1993), *Principles of Sediment Transport in Rivers, Estuaries and Coastal Seas*, Aqua, Amsterdam.

Venditti, J. G. (2003), The initiation and development of sand dunes in river channels, Ph.D. thesis, Univ. of B. C., Vancouver, B. C., Canada.

Venditti, J. G., and S. J. Bennett (2000), Spectral analysis of turbulent flow and suspended sediment transport over fixed dunes, *J. Geophys. Res.*, *105*, 22,035–22,047.

Venditti, J. G., M. A. Church, and S. J. Bennett (2005), Bed form initiation from a flat sand bed, *J. Geophys. Res.*, *110*, F01009, doi:10.1029/2004JF000149.

Villard, P. V., and M. Church (2003), Dunes and associated sand transport in a tidally influenced sand-bed channel: Fraser River, British Columbia, *Can. J. Earth Sci.*, *40*, 115–130.

Whiting, P. J., W. E. Dietrich, L. B. Leopold, T. G. Drake, and R. L. Shreve (1988), Bedload sheets in heterogeneous sediment, *Geology*, *16*, 105–108.

Yalin, M. S. (1964), Geometrical properties of sand waves, *J. Hydraul. Div. Am. Soc. Civil Eng.*, *90*, 105–109.

Yalin, M. S. (1977), *Mechanics of Sediment Transport*, Elsevier, New York.

Yalin, M. S. (1985), On the determination of ripple geometry, *J. Hydraul. Eng.*, *111*, 1148–1155.

S. J. Bennett, Department of Geography, State University of New York at Buffalo, Buffalo, NY 14261-0055, USA.

M. Church, Department of Geography, University of British Columbia, Vancouver, BC, Canada V6T 1Z2.

J. G. Venditti, Department of Earth and Planetary Sciences, University of California, Berkeley, CA 94720, USA. (jgvenditti@yahoo.ca)